



Subaru High- z Exploration of Low-Luminosity Quasars (SHELLQs). IX. Identification of two red quasars at $z > 5.6$

Nanako KATO,^{1,*} Yoshiki MATSUOKA,^{2,*} Masafusa ONOUE,³ Shuhei KOYAMA,²
Yoshiki TOBA ,^{2,4,5} Masayuki AKIYAMA,⁶ Seiji FUJIMOTO,^{7,8}
Masatoshi IMANISHI,^{9,10} Kazushi IWASAWA,¹¹ Takuma IZUMI,^{9,10}
Nobunari KASHIKAWA,¹² Toshihiro KAWAGUCHI,¹³ Chien-Hsiu LEE ,¹⁴
Takeo MINEZAKI,¹⁵ Tohru NAGAO,² Akatoki NOBORIGUCHI,¹ and
Michael A. STRAUSS¹⁶

¹Graduate School of Science and Engineering, Ehime University, 2-5 Bunkyo-cho, Matsuyama, Ehime 790-8577, Japan

²Research Center for Space and Cosmic Evolution, Ehime University, 2-5 Bunkyo-cho, Matsuyama, Ehime 790-8577, Japan

³Max Planck Institut für Astronomie, Königstuhl 17, D-69117 Heidelberg, Germany

⁴Department of Astronomy, Kyoto University, Kitashirakawa-Oiwake-cho, Sakyo-ku, Kyoto, Kyoto 606-8502, Japan

⁵Academia Sinica Institute of Astronomy and Astrophysics, 11F of Astronomy-Mathematics Building, AS/NTU, No.1, Section 4, Roosevelt Road, Taipei 10617, Taiwan

⁶Astronomical Institute, Tohoku University, 6-3 Aoba, Aramaki, Aoba-ku, Sendai, Miyagi 980-8578, Japan

⁷The Cosmic DAWN Center, University of Copenhagen, Vibenshuset, Lyngbyvej 2, DK-2100 Copenhagen, Denmark

⁸Niels Bohr Institute, University of Copenhagen, Lyngbyvej2, DK-2100, Copenhagen, Denmark

⁹National Astronomical Observatory of Japan, 2-21-1 Osawa, Mitaka, Tokyo 181-8588, Japan

¹⁰Department of Astronomical Science, Graduate University for Advanced Studies (SOKENDAI), 2-21-1 Osawa, Mitaka, Tokyo 181-8588, Japan

¹¹ICREA and Institut de Ciències del Cosmos, Universitat de Barcelona, IEEC-UB, Martí i Franquès, 1, 08028 Barcelona, Spain

¹²Department of Astronomy, School of Science, The University of Tokyo, 7-3-1 Hongo, Bunkyo-ku, Tokyo 113-0033, Japan

¹³Department of Economics, Management and Information Science, Onomichi City University, Onomichi, Hiroshima 722-8506, Japan

¹⁴National Optical Astronomy Observatory, 950 North Cherry Avenue, Tucson, AZ 85719, USA

¹⁵Institute of Astronomy, School of Science, The University of Tokyo, 2-21-1 Osawa, Mitaka, Tokyo 181-0015, Japan

¹⁶Princeton University Observatory, Peyton Hall, Princeton, NJ 08544, USA

*E-mail: kato@cosmos.phys.sci.ehime-u.ac.jp, yk.matsuoka@cosmos.ehime-u.ac.jp

Received 2020 May 30; Accepted 2020 July 11

Abstract

We present the first discovery of dust-reddened quasars (red quasars) in the high- z universe ($z > 5.6$). This is a result from the Subaru High- z Exploration of Low-Luminosity

Quasars (SHELLQs) project, which is based on the sensitive multi-band optical imaging data produced by the Hyper Suprime-Cam (HSC) Subaru Strategic Program survey. We identified four red quasar candidates from the 93 spectroscopically confirmed high- z quasars in the SHELLQs sample, based on detections in the Wide-field Infrared Survey Explorer (WISE) data at 3.4 and 4.6 μm (rest-frame $\sim 5000\text{--}6500\text{ \AA}$). The amount of dust reddening was estimated with spectral energy distribution (SED) fits over optical and mid-infrared wavelengths. Two of the four candidates were found to be red quasars with dust reddening of $E(B - V) > 0.1$. The remaining SHELLQs quasars without individual WISE detections are significantly fainter in the WISE bands and bluer than the red quasars, although we did detect them in the $W1$ band in a stacked image. We also conducted the same SED fits for high- z optically-luminous quasars, but no red quasar was found. This demonstrates the power of Subaru HSC to discover high- z red quasars, which are fainter than the limiting magnitudes of past surveys in the rest-frame ultraviolet, due to dust extinction.

Key words: early universe — galaxies: high-redshift — quasars: general

1 Introduction

High- z quasars (i.e., those with $z > 5.6$) are a useful probe to understand the process of reionization, and the formation and evolution of supermassive black holes (SMBHs) and their host galaxies in the early Universe. More than 200 high- z quasars have been discovered to-date, by the rest-frame ultraviolet (UV) surveys in all but a few cases (e.g., Fan et al. 2000, 2001, 2003, 2004, 2006; Goto 2006; Willott et al. 2007, 2009, 2010; Mortlock et al. 2009, 2011; Venemans et al. 2013, 2015; Bañados et al. 2014, 2016, 2018; Reed et al. 2015, 2017, 2019; Matsuoka et al. 2016, 2018a, 2018b, 2019a, 2019b; Jiang et al. 2016; Mazzucchelli et al. 2017; Yang et al. 2019a, 2019b; Wang et al. 2019). However, the nature of the individual objects is still poorly understood. For example, while Atacama Large Millimeter/submillimeter Array (ALMA) observations have revealed the presence of active star formation and abundant dust in the host galaxies (e.g., Venemans et al. 2012, 2016; Wang et al. 2013; Izumi et al. 2018, 2019), it is unknown to what extent the central quasar radiation is extinguished by the dust. This is a critical issue, since the previous rest-UV surveys are sensitive only to almost extinction-free quasars; indeed, a very luminous quasar with $M_{1450} \sim -28$ mag would become as faint as $z_{\text{AB}} > 24$ mag with $E(B - V) > 0.3$, and would not be selected even in our deep high- z quasar survey with Subaru Hyper Suprime-Cam (HSC; see below).

This paper focuses on dust-reddened quasars, so-called red quasars, in the high- z universe. Red quasars have a non-negligible amount of dust extinction, but are not completely obscured. In this paper, a red quasar means a quasar with color excess of $E(B - V) > 0.1$ (Glikman et al. 2012), when the broad-band spectral energy distribution (SED) is

fitted with a typical quasar template and the Small Magellanic Cloud (SMC) dust extinction law over the rest-frame UV/optical wavelengths. A red quasar is defined to have at least one broad emission line in the spectrum, and thus is different from type 2 quasars. Type 2 quasars are almost completely obscured in the UV/optical due to our nearly edge-on view of the dust torus, while the sightlines to red quasars may graze the dust torus, or may be obscured by the dust in the host galaxy. Red quasars have been selected using optical (e.g., Richards et al. 2003), optical/mid-infrared (IR) (e.g., Ross et al. 2015; Hamann et al. 2017), near-IR/radio (e.g., Glikman et al. 2004, 2007, 2012; Urrutia et al. 2009) and mid-IR techniques (e.g., Lacy et al. 2007, 2013; Glikman et al. 2018) at $z < 4$. Red quasars are currently not known at $z > 5.0$, primarily due to their faintness in the rest-frame UV (observed optical) wavelengths, and to the lack of a large sample of quasars at such high redshifts.

The nature of red quasars, in particular whether they represent a different stage of evolution from normal extinction-free quasars, is still unclear. It may be related to the triggering and subsequent transition of quasars—the well-known merger driven scenario suggests that major mergers of gas-rich galaxies first create an obscured starburst phase. Obscured active galactic nuclei (AGNs) are triggered at the same time, and may subsequently blow out the interstellar gas of the host galaxies, leading to unobscured quasars, and finally to star formation quenching (Sanders et al. 1988; Kauffmann & Haehnelt 2000; Hopkins et al. 2008). Red quasars may correspond to the above blowout phase (e.g., Glikman et al. 2012; Urrutia et al. 2009). Other mechanisms have also been suggested to trigger AGNs, such as disc instability (Mo et al. 1998; Cole et al. 2000; Bower et al. 2006; Lagos et al. 2008; Fanidakis et al. 2011), minor

mergers (Hernquist & Mihos 1995; De Robertis et al. 1998; Lagos et al. 2008), and gas feeding from ordinary stellar processes (Ciotti & Ostriker 2007). Red quasars may or may not represent a distinct stage of these processes. Constructing a large sample of red quasars at various redshifts and environments may help us to understand the physical conditions required to produce this population.

This is the ninth paper from the Subaru High- z Exploration of Low-Luminosity Quasars (SHELLQs) project (Matsuoka et al. 2016), based on the Subaru HSC survey data. We aim to identify red quasars from the HSC high- z quasars, with the aid of IR photometry from Wide-field Infrared Survey Explore (WISE; Wright et al. 2010). We compiled the optical, near-IR, and WISE (W1, W2) photometry of the quasars, and performed SED fitting to look for evidence of dust reddening. We note that even with the two WISE bands, we can trace the rest-frame spectral coverage only up to $\sim 6500 \text{ \AA}$, and cannot access the near-IR portion of a spectrum. As we already mentioned, given that the quasars were selected in the rest-frame UV, our study is sensitive only to modest amounts of extinction. Nonetheless, the unprecedented depth of the HSC survey has a potential of finding red quasars that were missed in the previous surveys.

This paper is structured as follows. We introduce the data and sample in section 2. In section 3, we perform image decomposition of blended WISE sources, and then broad-band SED fitting with a quasar template. Our results are discussed in section 4, and summarized in section 5. This paper adopts the cosmological parameters $H_0 = 70 \text{ km s}^{-1} \text{ Mpc}^{-1}$, $\Omega_M = 0.3$, and $\Omega_\Lambda = 0.7$. All magnitudes are presented in the AB system (Oke & Gunn 1983).

2 Data and sample

The SHELLQs project is based on the sensitive multi-band optical imaging data produced by the HSC Subaru Strategic Program (SSP) survey¹ (Aihara et al. 2018). The HSC is a wide-field optical imaging camera installed on the 8.2 m Subaru Telescope on the summit of Mauna Kea, and covers a 1.5° diameter field of view (Miyazaki et al. 2018; Komiyama et al. 2018; Kawanomoto et al. 2018; Furusawa et al. 2018). The HSC-SSP is an imaging survey with five broad-bands (g , r , i , z , and y) plus several narrow bands, and has three layers with different combinations of area and depth (Wide, Deep, and UltraDeep). The survey started in 2014 March, and will cover 1400 deg^2 in the Wide layer (Aihara et al. 2018) when completed. The 5σ depths for a point source are (g , r , i , z , y) = (26.5, 26.1, 25.9, 25.1, 24.4) mag in the Wide layer. The HSC data are processed

with a pipeline that measures the properties of all detected objects (Bosch et al. 2018).

The SHELLQs project has spectroscopically confirmed 93 low-luminosity quasars at $z > 5.6$ selected from the HSC data (Matsuoka et al. 2016, 2018a, 2018b, 2019a, 2019b). This includes the first low-luminosity quasar at $z > 7$ (Matsuoka et al. 2019a). The SHELLQs quasars were selected by a Bayesian probabilistic algorithm, and, like other high- z quasar surveys, do not include quasars whose colors are close to those of Galactic stars. More specifically, the quasars were initially selected as point sources satisfying:

$$z_{\text{PSF}} < 24.5, \sigma_z < 0.155, i_{\text{PSF}} - z_{\text{PSF}} > 1.5, \\ \text{and } z_{\text{PSF}} - z_{\text{CModel}} < 0.15 \quad (1)$$

or

$$y_{\text{PSF}} < 25.0, \sigma_y < 0.217, z_{\text{PSF}} - y_{\text{PSF}} > 0.8 \\ \text{and } y_{\text{PSF}} - y_{\text{CModel}} < 0.15. \quad (2)$$

Here m_{PSF} is the point spread function (PSF) magnitude measured by fitting the PSF model to a given source, while m_{CModel} is the CModel magnitude measured by fitting a PSF-convolved, weighted combination of exponential and de Vaucouleurs models to the source (Bosch et al. 2018). Equations (1) and (2) represent the criteria of i -band dropout and z -band dropout candidates, respectively, where σ_m is the error of the PSF magnitude. The Bayesian algorithm uses sky surface density and spectral models of high- z quasars and contaminating brown dwarfs, and calculates the probability (P_Q) of each source being a high- z quasar. We are carrying out a spectroscopic follow-up of those candidates meeting $P_Q > 0.1$. We are also carrying out multi-wavelength follow-up observations of the discovered quasars; Izumi et al. (2018, 2019) report the results from ALMA observations, and Onoue et al. (2019) present initial results from deep near-IR spectroscopy of several objects.

This paper uses WISE data to select red quasars. The WISE bands provide rest-frame spectral coverage at $> 3500 \text{ \AA}$, which is inaccessible with common JHK bands, for $z > 6$ sources. The WISE performed an all-sky imaging survey in the 3.4 (W1), 4.6 (W2), 12 (W3), and 22 (W4) μm bands, with angular resolutions of $6''.1$, $6''.4$, $6''.5$, and $12''.0$, respectively. The 5σ depths for a point source are (W1, W2, W3, W4) = (19.6, 19.3, 16.8, 14.7) AB mag.² In this study, we use the AllWISE Source Catalog.³ This catalog is

¹ (<https://hsc.mtk.nao.ac.jp/ssp/>).

² (http://wise2.ipac.caltech.edu/docs/release/allwise/expsup/sec2_3a.html).

³ (http://wise2.ipac.caltech.edu/docs/release/allwise/expsup/sec1_1.html).

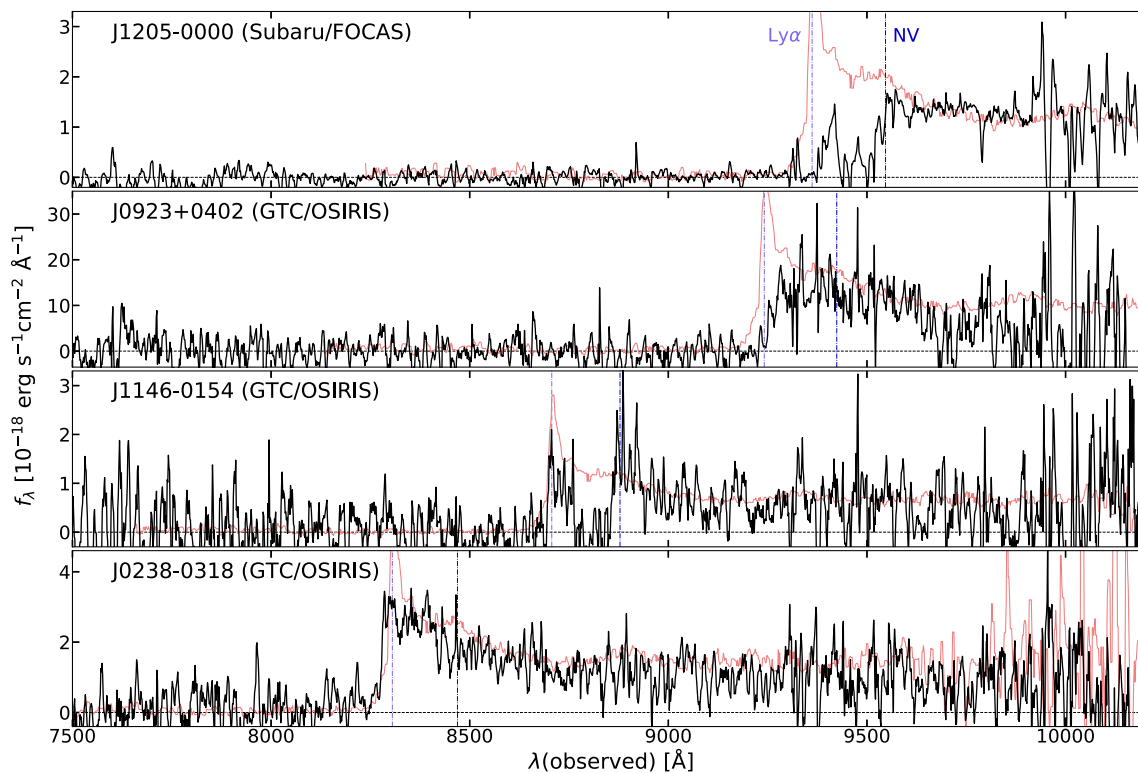


Fig. 1. Optical spectra (black line) of the red quasar candidates observed by Subaru/FOCAS or GTC/OSIRIS. The spectra were smoothed using inverse-variance weighted means over 5 pixels. The red line represents the stack spectrum of the SHELLQs quasars with unambiguous broad lines. The vertical lines represent the central wavelength of broad emission lines (Ly α : purple; N v: blue). J1205–0000 and J1146–0154 have BAL features bluewards of N v lines.

superior to the WISE All-Sky Release Catalog⁴ in the W1 and W2 bands, with improved photometric/astrometric accuracy. The magnitudes were converted from the Vega to AB system by adding 2.699 (W1), 3.339 (W2), 5.174 (W3), and 6.620 (W4) to the catalog values.⁵

We initially selected red quasar candidates by matching the SHELLQs sample to the WISE sources, with a matching radius of 3".0. Note that the W2 band is shallower by 0.3 mag than the W1, which is a good match to the color ($W1 - W2 = 0.3$) of a typical quasar spectrum (Selsing et al. 2016) with $E(B - V) = 0.1$. We found that four SHELLQs quasars—J120505.09–000027.9 (J1205–0000), J092347.12+040254.5 (J0923+0402), J114632.66–015438.2 (J1146–0154), and J023858.09–031845.4 (J0238–0318)—have WISE counterparts in the W1 and W2 bands ($S/N = 2$ –15), and regarded these four quasars as red quasar candidates for further analysis. Figure 1 displays their optical spectra, obtained with the Subaru/Faint Object Camera and Spectrograph (FOCAS; Kashikawa et al. 2002) or the Gran Telescopio Canarias (GTC)/Optical System for Imaging and low-Intermediate-Resolution Integrated Spectroscopy (OSIRIS; Cepa et al.

2000) (Matsuoka et al. 2016, 2018b, 2019b). We note that two of the four candidates, J1205–0000 and J1146–0154, have broad absorption line (BAL) features. In figure 2, we show the WISE images of the candidates. Table 1 presents their photometric and spectroscopic properties. None of the candidates are detected in the W3 or W4 bands. Note that, since the surface density of WISE sources in the HSC-Wide layer is $\sim 2.6 \text{ arcmin}^{-2}$, a single aperture with radius 3".0 would contain a WISE source by chance with $\sim 1.9\%$ probability. Thus the 93 quasars are expected to have 1.7 matched WISE objects purely by chance coincidence.

3 Analysis and results

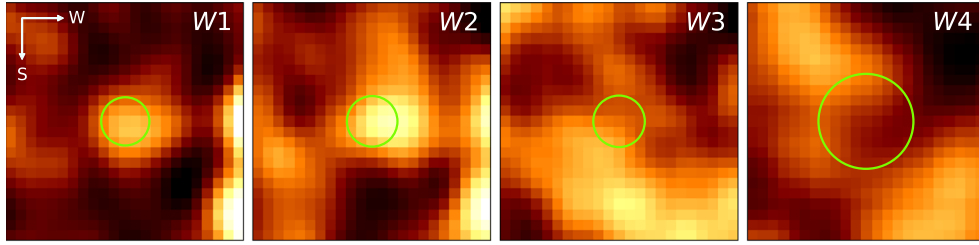
As shown in figures 3 and 4, we found neighbors around three quasars (J1205–0000, J0923+0402, and J1146–0154) in the HSC images, which may contribute to the AllWISE catalog fluxes. Therefore we modeled and decomposed the WISE images as a superposition of PSFs placed at the positions of the HSC detections. Here we assume that the neighbors are unresolved in WISE images, which indeed gives good fits to the observed WISE images, as we will see below.

To model the WISE PSFs, we mean-stacked ~ 10 bright and isolated point sources around each quasar found in the

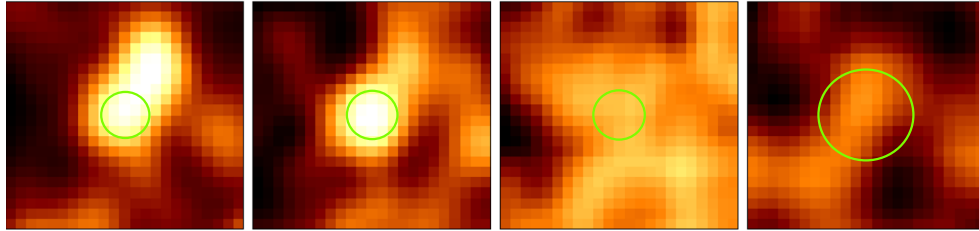
⁴ (<http://wise2.ipac.caltech.edu/docs/release/allsky>).

⁵ (http://wise2.ipac.caltech.edu/docs/release/allsky/expsup/sec4_4h.html).

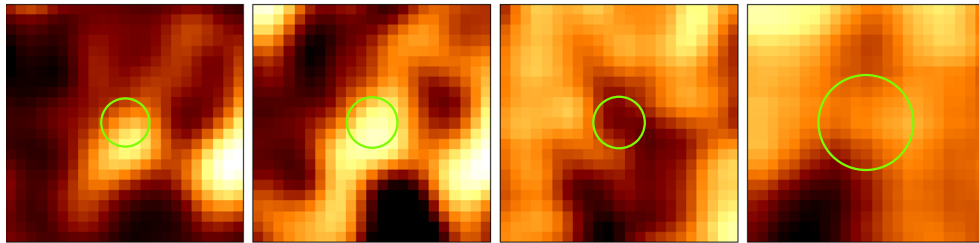
▷ J1205–0000



▷ J0923+0402



▷ J1146–0154



▷ J0238–0318

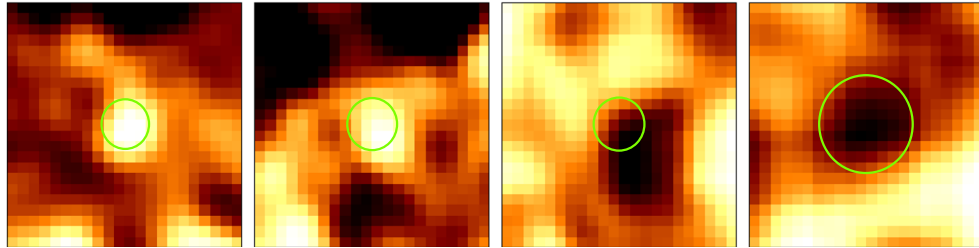


Fig. 2. WISE images of the red quasar candidates (W1, W2, W3, and W4 bands, from left to right). The image size is $30''$ on a side. The green circles indicate the angular resolution: $6''.1$, $6''.4$, $6''.5$, and $12''.0$ in W1, W2, W3, and W4, respectively.

WISE images, after normalizing the individual source profiles at the peak. We then superposed the scaled PSFs placed at the HSC positions of the quasar and neighbors, and performed χ^2 fitting to the observed WISE (W1, W2) images, looking for the best-fitting scaling parameters for the individual PSFs. We modeled the W1 and W2 images independently. The decomposed WISE quasar flux is then obtained by integrating the corresponding best-fitting PSF. Figure 5 presents the modeled WISE images of the three candidates. The decomposed flux errors were computed by combining in quadrature the AllWISE catalog flux errors (reflecting the background and calibration uncertainties) and the errors

coming from the decomposition process (which are of the order of $\sim 10\%$ of the flux), the latter being estimated from the χ^2 distributions. Since J0238–0318 has no neighbors that seem to contribute to its WISE flux (see the bottom right-hand panel of figure 4), we simply adopt its AllWISE catalog fluxes and errors.

The color excess $E(B - V)$ of the four quasars were estimated via broad-band SED fitting. We used the photometric data in the optical (HSC), near-IR, and mid-IR (WISE) bands. We do not use the W3- or W4-band information, since the relatively poor sensitivity does not allow us to give meaningful flux upper limits in these bands.

Table 1. Red quasar candidates.*

Object	i_{AB} (mag)	z_{AB} (mag)	y_{AB} (mag)	$W1_{AB}$ (mag)	$W2_{AB}$ (mag)	Redshift	M_{1450} (mag)	Ref. [†]
HSC J120505.09–000027.9	>26.72	>25.94	22.60 ± 0.03	19.98 ± 0.15	19.65 ± 0.23	6.70 [‡]	−24.56 ± 0.04	(1)
HSC J092347.12+040254.5	26.27 ± 0.20	22.64 ± 0.02	20.21 ± 0.01	19.06 ± 0.07	19.20 ± 0.16	6.60	−26.18 ± 0.14	(2)
HSC J114632.66–015438.2	26.57 ± 0.31	23.63 ± 0.06	23.78 ± 0.15	20.04 ± 0.16	20.16 ± 0.38	6.16	−23.43 ± 0.07	(2)
HSC J023858.09–031845.4	24.17 ± 0.08	22.64 ± 0.04	22.53 ± 0.08	20.57 ± 0.21	20.71 ± 0.50	5.83	−23.94 ± 0.03	(3)

*The coordinates are at J2000.0. The HSC coordinates are tied to the astrometric catalog from Gaia (Aihara et al. 2019). The HSC magnitudes (psfMag) were taken from the S18A internal data release. The magnitude lower limits are placed at 5σ significance. The WISE magnitudes were taken from the ALLWISE Source Catalog.

[†]References: (1) Matsuoka et al. (2018a), (2) Matsuoka et al. (2018b), (3) Matsuoka et al. (2019b).

[‡]The redshift of J1205–0000 was measured from the near-IR spectrum presented in Onoue et al. (2019) ($z = 6.699^{+0.007}_{-0.001}$).

The near-IR magnitudes were obtained from the VISTA Kilo-Degree Infrared Galaxy Survey (VIKING; Arnaboldi et al. 2007) and the UK Infrared Telescope Infrared Deep Sky Survey (UKIDSS; Lawrence et al. 2007) using a matching radius of $1''$ (see table 2). The near-IR surveys have the angular resolution of $\sim 1''$, and thus the quasar photometry is not affected by nearby objects. In principle, dust extinction makes a quasar spectrum flatter, while such flattening would also happen when there is a significant contribution from the host galaxy. We used two models for the SED fitting. The first model is a typical quasar template spectrum (Selsing et al. 2016) with the SMC extinction law (Hopkins et al. 2004); $R_V = 2.93$ is assumed (Pei 1992) (see section 4 for discussion on the choice of extinction laws). The second model is the same quasar template plus one of four galaxy templates (E, Im, Sbc, or Scd, taken from Coleman et al. 1980) representing the quasar host. The redshifts were fixed to the values in table 1, determined with spectroscopy, in the fitting.

Figure 6 presents the best-fitting SED and the estimated properties of each quasar. We present brief notes on the individual quasars in the following paragraphs. J1205–0000 and J0238–0318 have $E(B - V) > 0.1$ in the quasar plus dust extinction model, which gives better fits than the quasar plus galaxy model, and thus are identified as red quasars. J1146–0154 also has $E(B - V) > 0.1$, but we argue that its WISE counterpart may be a chance coincidence of a foreground source. Table 3 lists the best-fitting parameters of the four candidates.

J1205–0000: This is a z -band dropout source and the y -band flux is affected by intergalactic medium absorption, so we fitted the SED models to the VIKING J -, H -, and K_s -band fluxes and the decomposed $W1$ - and $W2$ -band fluxes. The quasar plus extinction model with $E(B - V) = 0.115^{+0.029}_{-0.027}$ gives a significantly better fit than the quasar plus galaxy model. In addition, the host galaxy inferred in the latter case ($M_{1450} \sim -23.0$ mag) is very luminous, given the characteristic magnitude of the $z \sim 7$ galaxy luminosity function ($M_{1450}^* \sim -20.8$ mag; Ono et al. 2018), but we found its HSC image to be consistent with a point source, without apparent contribution from the host galaxy (however, this is at the rest-frame $\sim 1400 \text{ \AA}$, and the situation can be different at $4000\text{--}6000 \text{ \AA}$ traced by the WISE bands). We concluded that the quasar plus extinction model is more reasonable, and that this object is a red quasar. A recently published near-IR spectrum of this quasar (Onoue et al. 2019) has a very flat continuum in rest-frame $2000\text{--}3000 \text{ \AA}$, consistent with our SED fitting result. We revisited the luminosity and black hole mass (M_{BH}) estimates given in Onoue et al. (2019), by taking into account the effect of dust extinction. As listed in table 4, the extinction-corrected AGN luminosity is almost twice the previous estimate,

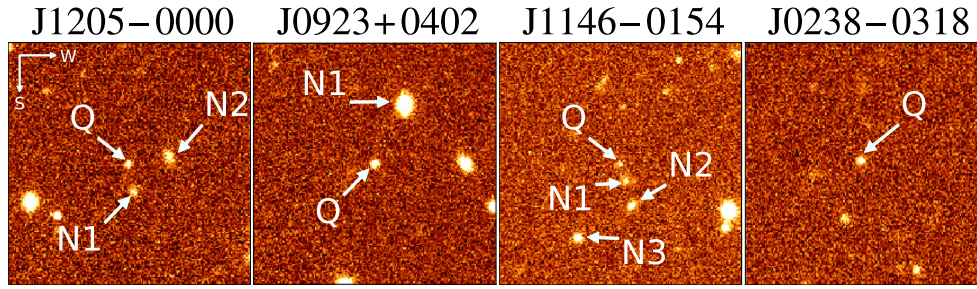


Fig. 3. HSC images of the red quasar candidates (y -band for J1205–0000, and z -band for the other three objects). The image size is $30''$ on a side. “Q” and “N” mark the quasar and nearby objects identified on the HSC images which could contribute to the AllWISE catalog flux. These are the HSC-Wide images with the 5σ limiting magnitudes of $y \sim 24.4$ mag (J1205–0000) and $z \sim 25.1$ mag (the remaining panels).

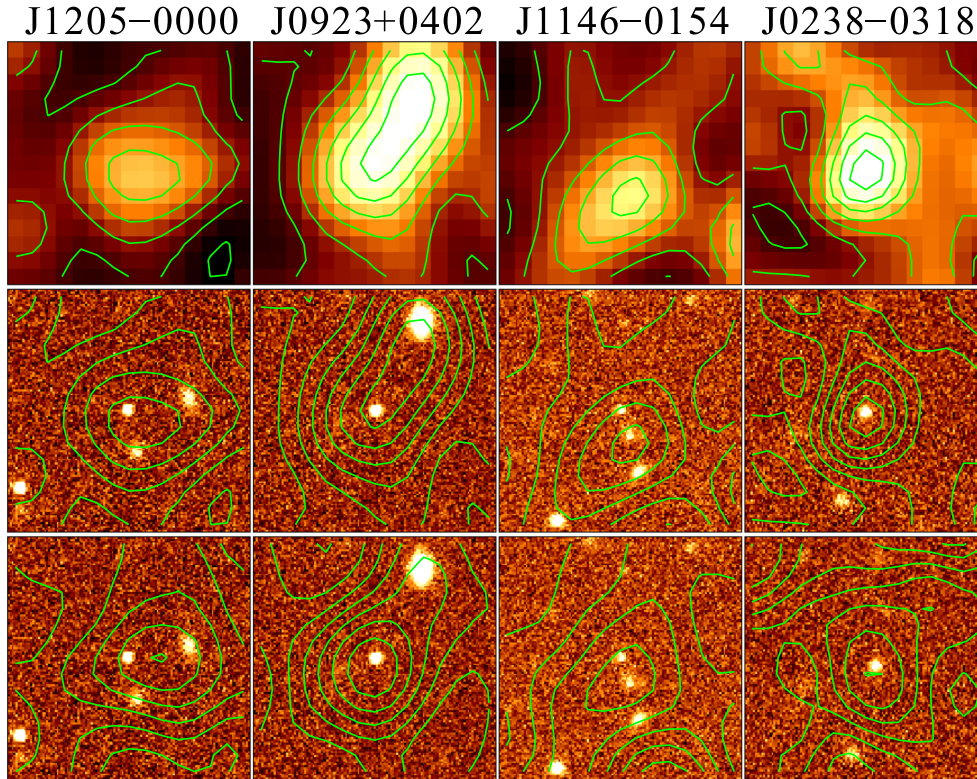


Fig. 4. $W1$ images (top) and HSC images with $W1/W2$ flux contours overlaid with green lines (middle/bottom) around the four red quasar candidates. The image size is $20''$ on a side. Note that the astrometric uncertainty of the WISE data is much smaller than the WISE PSF sizes.

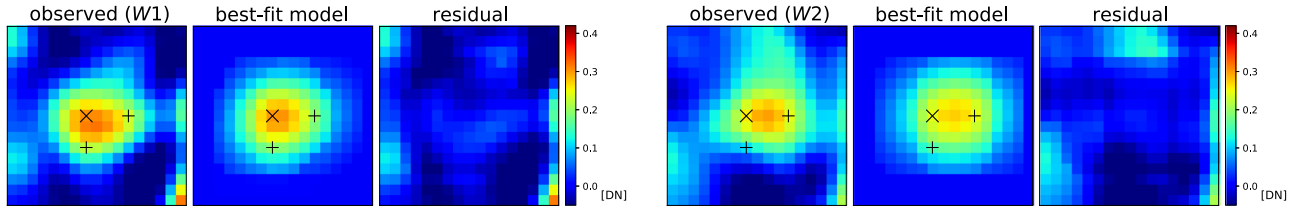
while the change of the M_{BH} and Eddington ratio is within the measurement errors. The near-IR spectrum shows a C IV BAL feature, but we confirm that it does not have a significant impact on the JHK_s photometry used for the SED fitting (see section 4).

J0923+0402: This is an i -band dropout source, and we fitted the SED models to the HSC y -band, UKIDSS J , H , K -band fluxes and the decomposed $W1$ - and $W2$ -band fluxes. The SED is reproduced by a quasar template without dust extinction, so J0923+0402 is a normal extinction-free quasar. This quasar is detected by WISE simply due to its

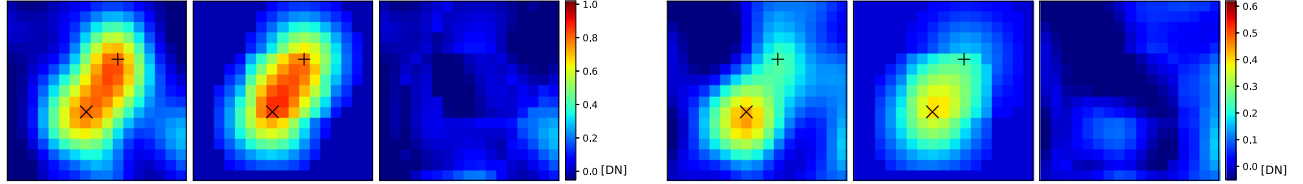
brightness; it is much brighter in the UV than the other three candidates (see table 1).

J1146–0154: This is an i -band dropout source and is not detected in the near-IR bands (the flux upper limits are given in figure 6), so we fitted the SED models to the HSC y -band flux and the decomposed $W1$ - and $W2$ -band fluxes. It is reasonably fitted by both the quasar plus extinction model with $E(B - V) = 0.162^{+0.020}_{-0.022}$ and the quasar plus galaxy model. Thus, it could be a red quasar. However, we noticed that the WISE flux decomposition is uncertain for this object. As shown in figure 4, the $W1$ flux peaks

▷ J1205–0000



▷ J0923+0402



▷ J1146–0154

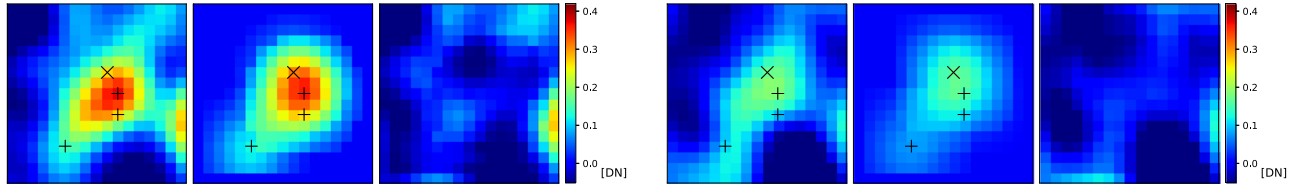


Fig. 5. WISE image decomposition. The left-hand part shows the observed image (left), the best-fitting model (middle), and the residual (right) in the *W1* band. The right-hand part shows those in the *W2* band. The cross and plus symbols represent the positions of the quasar and the neighbors, respectively. The image size is $23''$ on a side. J0238–0318 do not have neighbors contributing to the quasar WISE flux, and thus is not included here.

Table 2. IR magnitudes of the red quasar candidates.*

Object	J_{AB} (mag)	H_{AB} (mag)	K_{AB} (mag)	$W1_{AB}$ (mag)	$W2_{AB}$ (mag)
J1205–0000	21.95 ± 0.21^v	21.48 ± 0.34^v	20.73 ± 0.18^v	20.68 ± 0.18	20.47 ± 0.27
J0923+0402	20.02 ± 0.09^u	19.74 ± 0.16^u	19.32 ± 0.09^u	19.42 ± 0.08	19.68 ± 0.16
J1146–0154	$>22.15^v$	$>21.51^v$	$>21.45^v$	21.36 ± 0.21	20.92 ± 0.42
J0238–0318	20.57 ± 0.21	20.71 ± 0.50

*The IR magnitudes used in the SED fitting. The near-IR magnitudes (measured in $1''$ aperture radius) were taken from the VIKING (DR5,[†] labeled “v”) or UKIDSS (DR11,[‡] labeled “u”). The magnitude lower limits are placed at 5σ significance. The WISE magnitudes of J0238–0318 were taken from the AllWISE catalog, while those of the other candidates were derived with our image decomposition analysis (see text).

[†] (<http://horus.roe.ac.uk/vsa/index.html>).

[‡] (<http://wsa.roe.ac.uk/index.html>).

at the position of the neighbor N1, and the quasar contribution to the *W1* flux seems minor. Additionally, the *W1* and *W2* images are elongated in the E–W direction, while the quasar and nearby objects (N1 and N2) are arranged in the N–S direction in the HSC image. The decomposition may be more uncertain than reflected in the formal decomposed quasar flux errors, and so we do not include this object in the sample of red quasars in the following discussion. As we previously mentioned, one or two of our parent sample of 93 SHELLQs quasars could be matched to a foreground WISE source by chance, and this may be the case for J1146–0154.

J0238–0318: This is an *i*-band dropout source and is not observed in the near-IR bands. We fitted the SED models to the HSC γ -band flux and the AllWISE *W1*- and *W2*-band fluxes. The quasar plus extinction model with $E(B - V) = 0.127^{+0.018}_{-0.021}$ and the quasar plus galaxy model with a luminous host galaxy ($M_{1450} = -23.0$ mag) give similarly good fits. However, the χ^2 is smaller in the former case, and the host galaxy in the latter case becomes very luminous relative to the characteristic magnitude of the galaxy luminosity function at that redshift ($M_{1450}^* \sim -20.9$ mag; Ono et al. 2018). The source is not extended on the HSC image,

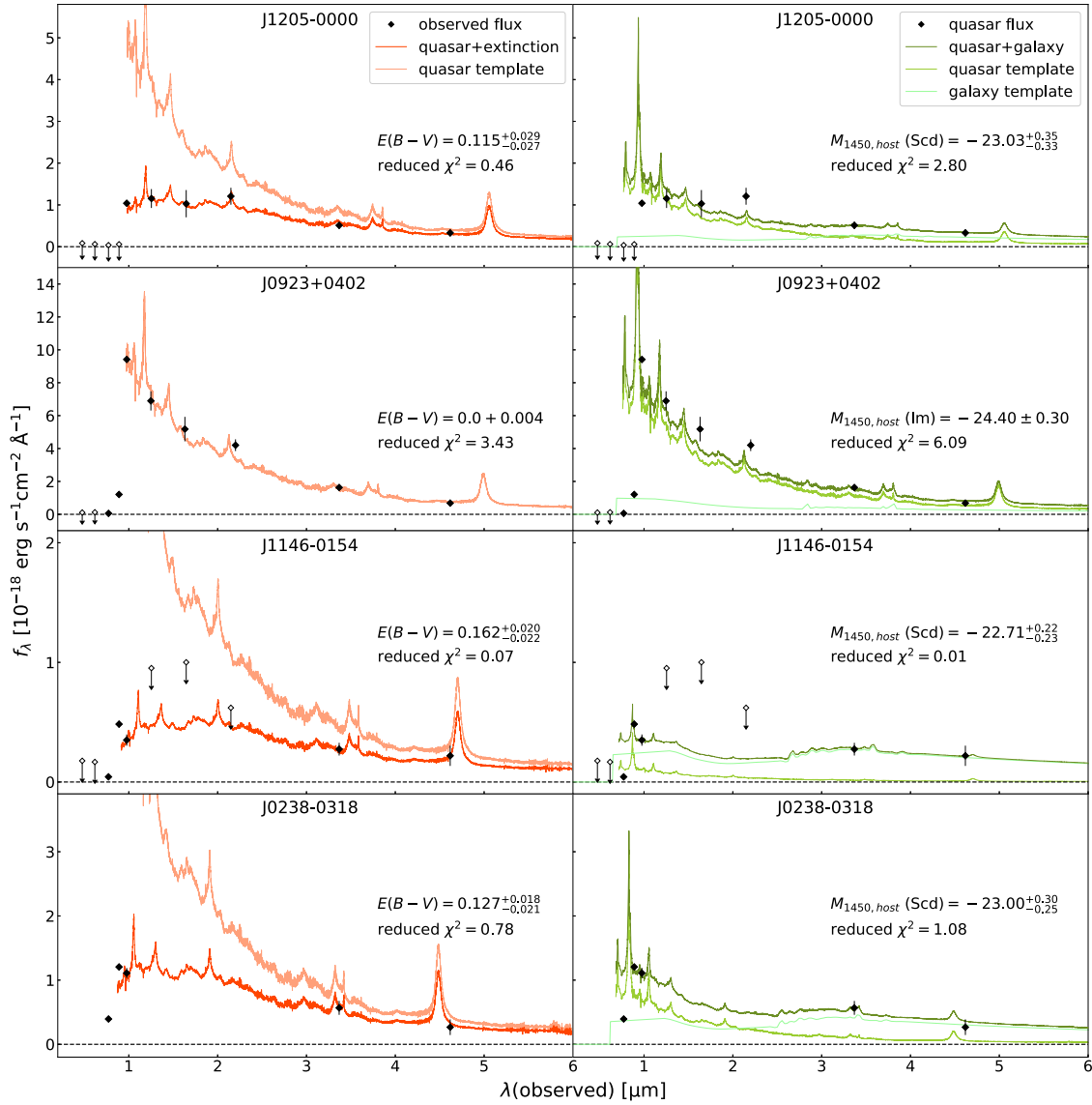


Fig. 6. SED fitting results. The observed fluxes and upper limits (5σ) are represented by the diamonds and arrows, respectively. The left-hand panels present the best-fitting quasar plus extinction model, along with the quasar template before the extinction is applied. The right-hand panels display the best-fitting quasar plus galaxy model, along with the individual quasar and galaxy templates. The color legend is given at the top right-hand corner of the top panels. We report the reduced χ^2 , $E(B-V)$, and the host galaxy luminosity in each panel.

Table 3. Best SED-fitting parameters of the red quasar candidates.

Object	Quasar plus extinction		Quasar plus galaxy
	$E(B-V)$ (mag)*	$M_{1450, \text{quasar}}$ (mag)	$M_{1450, \text{host}}$
J1205-0000	$0.115^{+0.029}_{-0.027}$	$-26.10^{+0.39}_{-0.36}$	$-23.03^{+0.35}_{-0.33}$
J0923+0402	$0.0 + 0.004$	$-26.18^{+0.15}_{-0.14}$	-24.40 ± 0.30
J1146-0154	$0.162^{+0.020}_{+0.022}$	$-25.61^{+0.28}_{-0.30}$	$-22.71^{+0.22}_{-0.23}$
J0238-0318	$0.127^{+0.018}_{-0.021}$	$-25.65^{+0.24}_{-0.28}$	$-23.00^{+0.30}_{-0.25}$

*Intrinsic quasar luminosity corrected for the dust extinction.

Table 4. Luminosity and black hole mass estimates of J1205-0000.

	Onoue et al. (2019)	Extinction-corrected
λL_{3000} (10^{45} erg s $^{-1}$)	8.96 ± 0.66	$16.15^{+2.68}_{-2.53}$
M_{BH} (M_{\odot}) ($10^9 M_{\odot}$)	$2.2^{+0.2}_{-0.6}$	$2.9^{+0.3}_{-0.8}$
$L_{\text{bol}}/L_{\text{Edd}}$	$0.16^{+0.04}_{-0.02}$	$0.22^{+0.04}_{-0.03}$

and has a typical spectrum of a high- z quasar in the rest-UV. We thus regard that the quasar plus extinction model is more reasonable, and that this object is a red quasar.

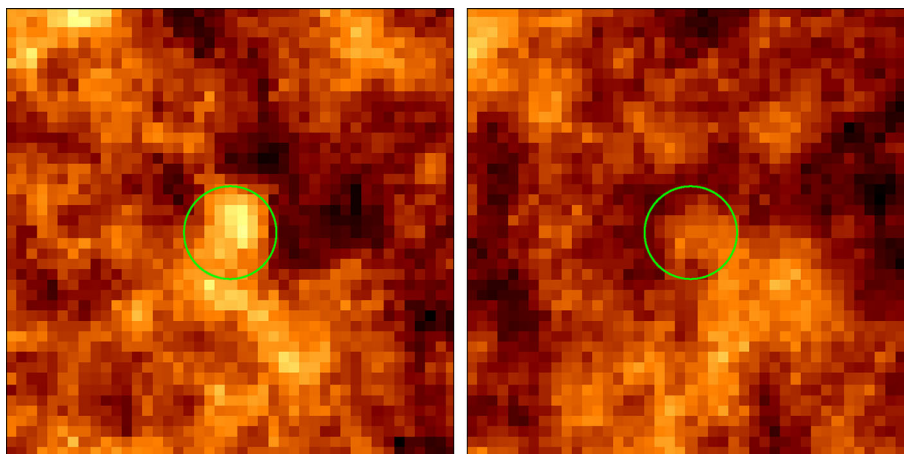


Fig. 7. Stacked images of the 89 SHELLQs quasars without individual WISE detection, in the *W1* (left) and *W2* (right) bands. The green circles indicate the apertures (the diameter is twice the resolution, $12''.2$ and $12''.8$ in *W1* and *W2*) used for photometry. The image size is $60''$ on a side.

4 Discussion

Of the 93 quasars discovered by SHELLQs, only four were detected by WISE. In order to investigate the mean properties of the remaining 89 quasars, we stacked their WISE images centered at the HSC quasar coordinates; we did not normalize the individual images and simply calculate pixel-by-pixel median values. We found a signal ($>3\sigma$) only in the *W1* stacked image, as displayed in figure 7. The aperture magnitude in the *W1*-band is 22.75 ± 0.40 mag, while the 3σ magnitude limit in the *W2*-band is >22.49 mag. The 89 quasars are significantly (>2 mag in *W1*) fainter than the two red quasars, as shown in figure 8 (top).

The mean broad-band SED of the 89 quasars is presented in figure 9. It is well fitted by the quasar template spectrum without dust extinction [i.e., $E(B - V) = 0.0$]. Indeed, the $y - W1$ ($= 0.60$) and $y - W2$ (< 1.0) colors of the mean SED are significantly bluer than the two red quasars, as shown in figure 8 (bottom). The above colors are close to the colors computed from the quasar template without extinction ($y - W1 = 0.61$ and $y - W2 = 0.77$). Thus, we concluded that the majority of the 89 quasars do not belong to the red quasar population.

For comparison with the SHELLQs low-luminosity quasars, we conducted the same analysis as described in section 3 for more luminous quasars. We started from the compilation in Bañados et al. (2016), who listed all the high- z quasars known before 2016 March. The 87 quasars detected by the Panoramic Survey Telescope & Rapid Response System1 (Pan-STARRS1, PS1; Chambers et al. 2016) and WISE (*W1* and *W2* bands) were picked up among the 164 objects. Excluding several problematic cases with very bright neighbors or irregular WISE source shapes, we have 80 luminous ($M_{1450} < -25.4$ mag) quasars for the following analysis.

Of the 80 luminous quasars, 40 have neighbors possibly contributing to the WISE flux, identified in the optical images. We performed WISE image decomposition using the approach described above. The coordinates of the neighbors were taken from the PS1 images. We fitted the same SED models as described above to the photometry data in the PS1 y -band, J -band, and the *W1*- and *W2*-bands; the y - and J -band magnitudes were taken from Bañados et al. (2016), where the J -band magnitudes were compiled from various papers. Four quasars were best-fitted with SEDs with $E(B - V) = 0.05 - 0.1$, while all the remaining quasars have $E(B - V) < 0.05$, and thus no red quasar was found. In some cases we found that the quasar plus galaxy model gives a good fit, but further investigation of the possible host contribution in the luminous quasars is beyond the scope of the present analysis.

Figure 10 compares the results for the luminous sample with those for the SHELLQs quasars. Red quasars are found only among the low-luminosity objects with $M_{1450} > -25$ mag, and the intrinsic luminosity (i.e., prior to being affected by dust extinction) of the red quasars are around the lower envelope of the luminous quasars. The fraction of red quasars in the SHELLQs sample is $\sim 2.2\%$ ($2/93$), and if we assume the same fraction at the luminous side, we would expect to find four red quasars in the 164 luminous objects. We found no luminous red quasar in reality, which would happen with $\sim 3\%$ probability based on the Poisson statistics. Thus the red quasar fraction may get smaller as the observed quasar luminosity increases, but this is still inconclusive due to the small-number statistics. Having said that, there may be two possible reasons why we do not see red quasars in the luminous sample. A red quasar in the luminous sample would have an even brighter unextincted M_{1450} than measured, but the number density of

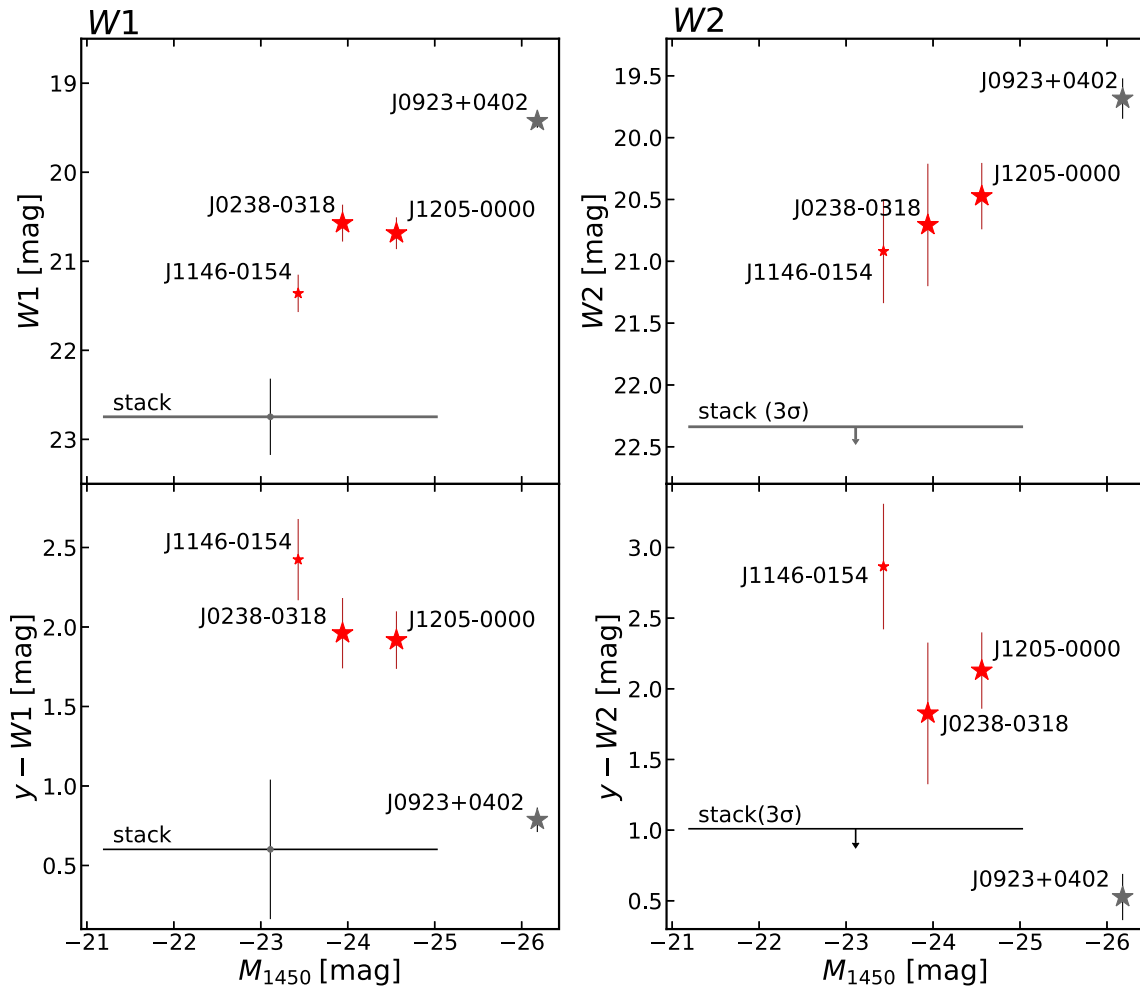


Fig. 8. UV absolute magnitudes (M_{1450}) versus the WISE magnitudes (top) and $\gamma - \text{WISE}$ colors (bottom) ($W1$ on the left and $W2$ on the right). The stars represent the four SHELLQs quasars with WISE detection. The three quasars with $E(B - V) > 0.1$ are marked in red, while the WISE image decomposition for J1146–0154 (small star) is considered uncertain; see text. The horizontal lines represent the stacking results for the remaining 89 quasars; the arrows represent 3σ upper limits.

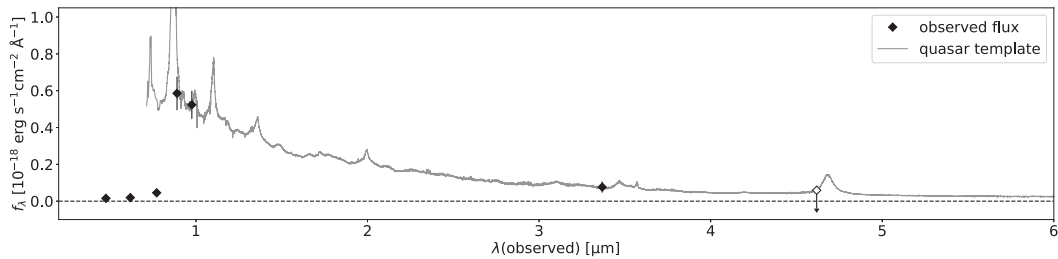


Fig. 9. Comparison of the quasar template spectrum (Selsing et al. 2016) with the mean broad-band SED of the 89 SHELLQs quasars without individual WISE detection. The optical data (HSC- g, r, i, z, y) represent the median magnitudes of the 89 quasars, while the $W1$ and $W2$ data are the result of stacking. The arrow in the $W2$ -band represents the 3σ upper limit. The quasar template was normalized to the observed y -band flux, and was drawn at the median redshift ($z = 6.13$) of the 89 quasars.

high- z quasars drops steeply above $M_{1450} \sim -25$ mag (Matsuoka et al. 2018c), and hence high- z quasars with such brightest magnitudes are very rare. Alternatively, it is also possible that red quasars are rarer at higher lumi-

nosity as a result of some physical mechanisms; for example, stronger effects of AGN feedback may quickly blow out the surrounding material, resulting in a shorter timescale in which they can be observed as red quasars.

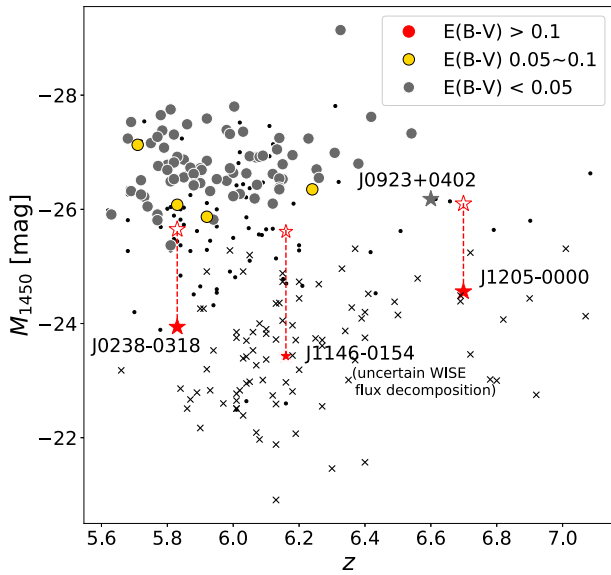


Fig. 10. Rest-UV absolute magnitudes at 1450 \AA (M_{1450}) of the four SHELLQs quasars (filled stars) and the 80 luminous quasars (filled circles) with WISE detection, as a function of redshift. The colors of the points represent the amount of inferred dust extinction, as indicated at the top right-hand corner. The open stars represent the extinction-corrected M_{1450} for the SHELLQs red quasars. For reference, we also plot the SHELLQs quasars (crosses) and the luminous quasars in Bañados et al. (2016, dots) which are not analyzed in the present work, due mostly to non-detection in the WISE bands.

Overall, the observed fraction of high- z red quasars seems very low. Indeed, previous studies found the fraction at lower redshifts to be between $\sim 15\%$ and $\sim 30\%$ (Richards et al. 2003; Glikman et al. 2004, 2012, 2018; Lacy et al. 2007, 2013). Richards et al. (2003) have reported a fraction of $\simeq 15\%$ among ~ 4500 quasars with $0.3 \leq z \leq 2.2$ in the Sloan Digital Sky Survey (SDSS; York et al. 2000), while Glikman et al. (2012) have estimated the fraction of $\sim 15\%$ – 20% in the radio/near-IR selected sample at $0.13 < z < 3.1$. However, it is not straightforward to compare the red quasar fraction at high- z and low- z directly, due to various systematic differences in the selection, luminosity, and definition of a red quasar, among other factors. In particular, the present estimates at high- z may be biased toward a lower value, because they are based on the rest-UV surveys, which may have missed a significant population of dust-extincted quasars.

In the SED fitting procedure, we adopted the SMC extinction law in accordance with the previous studies (Richards et al. 2003; Glikman et al. 2004, 2012; Hopkins et al. 2004), since the low metallicity of the SMC is expected to be close to the environment in high- z galaxies (see also, Maiolino et al. 2004; Gallerani et al. 2010). In order to assess the dependence of our results on the extinction law, we repeated the SED fitting with the extinction laws of the Large Magellanic Cloud (LMC) with $R_V = 3.16$,

the Milky Way (Pei 1992) with $R_V = 3.08$, and starburst galaxies (Calzetti et al. 2000) with $R_V = 3.1$. The $E(B - V)$ values of the two red quasars are 0.117, 0.139, 0.176, and 0.321 for J1205–0000, and 0.127, 0.165, 0.256, and 0.458 for J0238–0318, with the extinction laws of SMC, LMC, the Milky Way, and starbursts, respectively. The results are consistent with the trend reported in Glikman et al. (2012), that the SMC extinction law gives the lowest $E(B - V)$ values. Thus J1205–0000 and J0238–0318 are classified as red quasars regardless of the choice of extinction law.

One concern is about quasar variability, as the HSC images were taken several years after the WISE observations. However, the time interval is actually less than a year at $z > 6$, and the expected variability at the rest-frame $\sim 1200 \text{ \AA}$ (traced by the HSC z/y band) is $\sim 0.2 \text{ mag}$ for the luminosity of our quasars (Kimura et al. 2020). We confirmed that this level of variability does not affect our results, in particular the classification of J1205–0000 and J0238–0318 into red quasars.

Finally, we note that the rest-frame UV spectra of J1205–0000 and J1146–0154 have BAL features (see figure 1). BAL features are thought to be generated by gas outflow ejected at high velocities from the vicinity of a quasar. The BAL fraction among the full quasars population at $z \lesssim 4$ is estimated to be $\sim 10\%$ – 15% (e.g., Tolea et al. 2002; Hewett & Foltz 2003; Reichard et al. 2003b; Gibson et al. 2009). Some previous studies suggested the redshift dependence of the BAL quasar fraction (Tolea et al. 2002; Allen et al. 2011). Indeed, Wang et al. (2019) found that the BAL fraction at $z \gtrsim 6.5$ is $\gtrsim 22\%$, which is a little higher than that at lower redshift. It is known that BAL quasars, especially low-ionization BALs, are redder than general quasars (Sprayberry & Foltz 1992). It has also been reported that red quasars have a large BAL fraction. Richards et al. (2003) found that the fraction is 20% among 96 dust-reddened quasars in the SDSS at $1.7 \leq z \leq 2.2$. Urrutia et al. (2009) estimated the conservative BAL fraction of 37% for their radio/near-IR selected 19 quasars at $z > 0.9$. Dai, Shankar, and Sivakoff (2008) suggest that quasar samples selected in the near-IR have a larger BAL fraction than those selected in the optical. In our two confirmed red quasars (J1205–0000 and J0238–0318), at least one has a BAL feature. Of course this is a small sample, and a larger sample is needed to provide statically meaningful results. Having said that, our results might indicate that high- z red quasars are also preferentially associated with BAL. The large BAL fraction would indicate that red quasars are in the dust- and gas-enshrouded phase of quasar evolution, with outflows that may eventually blow out the surrounding materials.

Since BAL may affect the broad-band magnitudes used above, we repeated SED fitting by replacing the Selsing et al. (2016) quasar template with a BAL template provided by Hamann et al. (2019, their high-ionization BALs (HiBALs) template in figure 5). Since the BAL template only covers the rest-frame wavelengths $<3000 \text{ \AA}$, we kept using the Selsing et al. (2016) template at $3000\text{--}6500 \text{ \AA}$, where no strong absorption is present in HiBAL quasars. When corrected for the intrinsic extinction of $E(B - V) \sim 0.023$ in the BAL template (Reichard et al. 2003a, 2003b), our two BAL quasars have $E(B - V) = 0.111^{+0.028}_{-0.027}$ (J1205–0000) and $0.158^{+0.021}_{-0.023}$ (J1146–0154). Thus J1205–0000 remains a red quasar, and our conclusions remain the same.

5 Summary

This paper presented the discovery of two dust-reddened quasars among the 93 SHELLQs quasars. We pre-selected four candidates based on the WISE detection in the W1- and W2-bands, and performed SED fitting to see whether the candidates meet the red quasar definition, $E(B - V) \geq 0.1$, following Glikman et al. (2012). Of the four red quasar candidates, three have bright neighbors in the HSC images. Because these neighbors could contribute to the AllWISE catalog fluxes, we modeled and decomposed the WISE images as a superposition of PSFs. We used two different models for the SED fitting; a typical quasar template with the SMC extinction law, and the same quasar template with one of four empirical galaxy templates. As a result, we found that two quasars, J1205–0000 and J0238–0318, are red quasars. We found that the remaining 89 SHELLQs quasars without individual WISE detections are significantly fainter in the WISE bands and bluer than the red quasars, and have a mean (stacked) spectrum consistent with an extinction-free quasar template. We also carried out the same analysis for 80 luminous quasars at $z > 5.6$ taken from Bañados et al. (2016), but no red quasar was found. This demonstrates the power of the wide and deep survey by HSC, which enabled us to identify high- z red quasars for the first time.

The number of high- z red quasars is still insufficient to statistically discuss their properties. We will continue to search for high- z red quasars, with the progress of the HSC-SSP survey. In the short term, we plan to pursue the possibility of using the *Spitzer* Infrared Array Camera data with better angular resolution and sensitivity than WISE, though the analysis would be limited to the HSC Deep fields. Future large projects such as the Rubin Observatory Legacy Survey of Space and Time in the optical and Euclid in the near-IR would be useful to further advance surveys for red quasars, while deep follow-up observations with the Thirty Meter Telescope, the James Webb Space Telescope,

and other facilities would play critical roles in studying their individual nature in detail.

Acknowledgments

We are grateful to the referee for his/her useful comments to improve this paper. YM was supported by the Japan Society for the Promotion of Science (JSPS) KAKENHI grant No. JP17H04830 and the Mitsubishi Foundation grant No. 30140. TI acknowledges supports from the JSPS grant No. JP17K14247.

The Hyper Suprime-Cam (HSC) collaboration includes the astronomical communities of Japan and Taiwan, and Princeton University. The HSC instrumentation and software were developed by the National Astronomical Observatory of Japan (NAOJ), the Kavli Institute for the Physics and Mathematics of the Universe (Kavli IPMU), the University of Tokyo, the High Energy Accelerator Research Organization (KEK), the Academia Sinica Institute for Astronomy and Astrophysics in Taiwan (ASIAA), and Princeton University. Funding was contributed by the FIRST program from Japanese Cabinet Office, the Ministry of Education, Culture, Sports, Science and Technology (MEXT), the Japan Society for the Promotion of Science (JSPS), Japan Science and Technology Agency (JST), the Toray Science Foundation, NAOJ, Kavli IPMU, KEK, ASIAA, and Princeton University.

The Pan-STARRS1 Surveys (PS1) have been made possible through contributions of the Institute for Astronomy, the University of Hawaii, the Pan-STARRS Project Office, the Max-Planck Society and its participating institutes, the Max Planck Institute for Astronomy, Heidelberg and the Max Planck Institute for Extraterrestrial Physics, Garching, The Johns Hopkins University, Durham University, the University of Edinburgh, Queen's University Belfast, the Harvard-Smithsonian Center for Astrophysics, the Las Cumbres Observatory Global Telescope Network Incorporated, the National Central University of Taiwan, the Space Telescope Science Institute, the National Aeronautics and Space Administration under Grant No. NNX08AR22G issued through the Planetary Science Division of the NASA Science Mission Directorate, the National Science Foundation under Grant No. AST-1238877, the University of Maryland, and Eotvos Lorand University (ELTE).

This paper makes use of software developed for the Large Synoptic Survey Telescope. We thank the LSST Project for making their code available as free software at (<http://dm.lsst.org>).

This publication makes use of data products from the Wide-field Infrared Survey Explorer, which is a joint project of the University of California, Los Angeles, and the Jet Propulsion Laboratory/California Institute of Technology, funded by the National Aeronautics and Space Administration.

References

- Aihara, H., et al. 2018, PASJ, 70, S4
- Aihara, H., et al. 2019, PASJ, 71, 114
- Allen, J. T., Hewett, P. C., Maddox, N., Richards, G. T., & Belokurov, V. 2011, MNRAS, 410, 860
- Arnaboldi, M., Neeser, M. J., Parker, L. C., Rosati, P., Lombardi, M., Dietrich, J. P., & Hummel, W. 2007, Messenger, 127, 28
- Bañados, E., et al. 2014, AJ, 148, 14
- Bañados, E., et al. 2016, ApJS, 227, 11
- Bañados, E., et al. 2018, ApJ, 856, L25
- Bosch, J., et al. 2018, PASJ, 70, S5

- Bower, R. G., Benson, A. J., Malbon, R., Helly, J. C., Frenk, C. S., Baugh, C. M., Cole, S., & Lacey, C. G. 2006, *MNRAS*, 370, 645
- Calzetti, D., Armus, L., Bohlin, R. C., Kinney, A. L., Koornneef, J., & Storchi-Bergmann, T. 2000, *ApJ*, 533, 682
- Cepa, J., et al. 2000, *Proc. SPIE*, 4008, 623
- Chambers, K. C., et al. 2016, *arXiv:1612.05560*
- Ciotti, L., & Ostriker, J. P. 2007, *ApJ*, 665, 1038
- Cole, S., Lacey, C. G., Baugh, C. M., & Frenk, C. S. 2000, *MNRAS*, 319, 168
- Coleman, G. D., Wu, C.-C., & Weedman, D. W. 1980, *ApJS*, 43, 393
- Dai, X., Shankar, F., & Sivakoff, G. R. 2008, *ApJ*, 672, 108
- De Robertis, M. M., Yee, H. K. C., & Hayhoe, K. 1998, *ApJ*, 496, 93
- Fan, X., et al. 2000, *AJ*, 120, 1167
- Fan, X., et al. 2001, *AJ*, 122, 2833
- Fan, X., et al. 2003, *AJ*, 125, 1649
- Fan, X., et al. 2004, *AJ*, 128, 515
- Fan, X., et al. 2006, *AJ*, 131, 1203
- Fanidakis, N., Baugh, C. M., Benson, A. J., Bower, R. G., Cole, S., Done, C., & Frenk, C. S. 2011, *MNRAS*, 410, 53
- Furusawa, H., et al. 2018, *PASJ*, 70, S3
- Gallerani, S., et al. 2010, *A&A*, 523, A85
- Gibson, R. R., et al. 2009, *ApJ*, 692, 758
- Glikman, E., et al. 2012, *ApJ*, 757, 51
- Glikman, E., et al. 2018, *ApJ*, 861, 37
- Glikman, E., Gregg, M. D., Lacy, M., Helfand, D. J., Becker, R. H., & White, R. L. 2004, *ApJ*, 607, 60
- Glikman, E., Helfand, D. J., White, R. L., Becker, R. H., Gregg, M. D., & Lacy, M. 2007, *ApJ*, 667, 673
- Goto, T. 2006, *MNRAS*, 371, 769
- Hamann, F., et al. 2017, *MNRAS*, 464, 3431
- Hamann, F., Herbst, H., Paris, I., & Capellupo, D. 2019, *MNRAS*, 483, 1808
- Hernquist, L., & Mihos, J. C. 1995, *ApJ*, 448, 41
- Hewett, P. C., & Foltz, C. B. 2003, *AJ*, 125, 1784
- Hopkins, P. F., et al. 2004, *AJ*, 128, 1112
- Hopkins, P. F., Hernquist, L., Cox, T. J., & Kereš, D. 2008, *ApJS*, 175, 356
- Izumi, T., et al. 2018, *PASJ*, 70, 36
- Izumi, T., et al. 2019, *PASJ*, 71, 111
- Jiang, L., et al. 2016, *ApJ*, 833, 222
- Kashikawa, N., et al. 2002, *PASJ*, 54, 819
- Kauffmann, G., & Haehnelt, M. 2000, *MNRAS*, 311, 576
- Kawanomoto, S., et al. 2018, *PASJ*, 70, 66
- Kimura, Y., Yamada, T., Kokubo, M., Yasuda, N., Morokuma, T., Nagao, T., & Matsuoka, Y. 2020, *ApJ*, 894, 24
- Komiyama, Y., et al. 2018, *PASJ*, 70, S2
- Lacy, M., et al. 2013, *ApJS*, 208, 24
- Lacy, M., Petric, A. O., Sajina, A., Canalizo, G., Storrie-Lombardi, L. J., Armus, L., Fadda, D., & Marleau, F. R. 2007, *AJ*, 133, 186
- Lagos, C. D. P., Cora, S. A., & Padilla, N. D. 2008, *MNRAS*, 388, 587
- Lawrence, A., et al. 2007, *MNRAS*, 379, 1599
- Maiolino, R., Schneider, R., Oliva, E., Bianchi, S., Ferrara, A., Mannucci, F., Pedani, M., & Roca Sogorb, M. 2004, *Nature*, 431, 533
- Matsuoka, Y., et al. 2016, *ApJ*, 828, 26
- Matsuoka, Y., et al. 2018a, *PASJ*, 70, S35
- Matsuoka, Y., et al. 2018b, *ApJS*, 237, 5
- Matsuoka, Y., et al. 2018c, *ApJ*, 869, 150
- Matsuoka, Y., et al. 2019a, *ApJ*, 872, L2
- Matsuoka, Y., et al. 2019b, *ApJ*, 883, 183
- Mazzucchelli, C., et al. 2017, *ApJ*, 849, 91
- Miyazaki, S., et al. 2018, *PASJ*, 70, S1
- Mo, H. J., Mao, S., & White, S. D. M. 1998, *MNRAS*, 295, 319
- Mortlock, D. J., et al. 2009, *A&A*, 505, 97
- Mortlock, D. J., et al. 2011, *Nature*, 474, 616
- Oke, J. B., & Gunn, J. E. 1983, *ApJ*, 266, 713
- Ono, Y., et al. 2018, *PASJ*, 70, S10
- Onoue, M., et al. 2019, *ApJ*, 880, 77
- Pei, Y. C. 1992, *ApJ*, 395, 130
- Reed, S. L., et al. 2015, *MNRAS*, 454, 3952
- Reed, S. L., et al. 2017, *MNRAS*, 468, 4702
- Reed, S. L., et al. 2019, *MNRAS*, 487, 1874
- Reichard, T. A., et al. 2003a, *AJ*, 125, 1711
- Reichard, T. A., et al. 2003b, *AJ*, 126, 2594
- Richards, G. T., et al. 2003, *AJ*, 126, 1131
- Ross, N. P., et al. 2015, *MNRAS*, 453, 3932
- Sanders, D. B., Soifer, B. T., Elias, J. H., Madore, B. F., Matthews, K., Neugebauer, G., & Scoville, N. Z. 1988, *ApJ*, 325, 74
- Selsing, J., Fynbo, J. P. U., Christensen, L., & Krogager, J.-K. 2016, *A&A*, 585, A87
- Sprayberry, D., & Foltz, C. B. 1992, *ApJ*, 390, 39
- Tolea, A., Krolik, J. H., & Tsvetanov, Z. 2002, *ApJ*, 578, L31
- Urrutia, T., Becker, R. H., White, R. L., Glikman, E., Lacy, M., Hodge, J., & Gregg, M. D. 2009, *ApJ*, 698, 1095
- Venemans, B. P., et al. 2012, *ApJ*, 751, L25
- Venemans, B. P., et al. 2013, *ApJ*, 779, 24
- Venemans, B. P., et al. 2015, *MNRAS*, 453, 2259
- Venemans, B. P., Walter, F., Zschaechner, L., Decarli, R., De Rosa, G., Findlay, J. R., McMahon, R. G., & Sutherland, W. J. 2016, *ApJ*, 816, 37
- Wang, F., et al. 2019, *ApJ*, 884, 30
- Wang, R., et al. 2013, *ApJ*, 773, 44
- Willott, C. J., et al. 2007, *AJ*, 134, 2435
- Willott, C. J., et al. 2009, *AJ*, 137, 3541
- Willott, C. J., et al. 2010, *AJ*, 139, 906
- Wright, E. L., et al. 2010, *AJ*, 140, 1868
- Yang, J., et al. 2019a, *AJ*, 157, 236
- Yang, J., et al. 2019b, *ApJ*, 871, 199
- York, D. G., et al. 2000, *AJ*, 120, 1579